The Influence of Sea Surface Temperature Gradients on Stratiform Cloudiness along the Equatorial Front in the Pacific Ocean

CLARA DESER,* JOHN J. BATES,+ AND SUSAN WAHL*

*CIRES, University of Colorado, Boulder, Colorado
+Climate Research Division, NOAA/ERL, Boulder, Colorado

(Manuscript received 10 August 1992, in final form 19 August 1992)

ABSTRACT

Satellite observations of visible cloudiness and sea surface temperature (SST) are used to test the hypothesis that the configuration of cool low-level winds blowing across a sharp SST front in the equatorial eastern Pacific gives rise to stratiform clouds on the warm (downstream) side of the front. The results show that there is a maximum in low clouds over the equatorial front during the cold season of 1988 when the front and cross-isotherm winds were strong. The low-cloud maximum was reduced in the warm El Niño year of 1987, consistent with the weakening of the front. Instability waves along the equatorial front were pronounced during the summer and autumn of 1988. The results show a strong association between visible cloud and the SST waves, with enhanced (reduced) cloudiness in the warm troughs (cold crests) of the waves.

1. Introduction

The equatorial front is a zone of strong meridional gradients in sea surface temperature (SST) centered a few degrees north of the equator in the eastern Pacific Ocean. The front is present throughout the year, reaching its greatest intensity in northern summer and autumn (Hayes et al. 1989). Climatological mean SST gradients along the front are on the order of 1°C (100 km)$^{-1}$ during the months of July through November (Fig. 1). The surface winds blow northward across the front from the cold side to the warm side, crossing the surface isotherms at nearly right angles (Fig. 1). The low-level air accelerates across the front, producing surface wind divergences on the order of 4×10^{-6} s^{-1} between the equator and ~4°N (Deser and Wallace 1990).

As cool air flows across the front, heat and moisture are rapidly fluxed into the atmospheric boundary layer. These sea-to-air fluxes destabilize the atmospheric mixed layer and lead to a reduction of the low-level wind shear on the warm side of the front (Bond 1992). Wallace et al. (1989) and Hayes et al. (1989) have suggested that the acceleration of the surface winds across the front may be due in part to the reduced static stability.

The vigorous fluxes of latent and sensible heat over the front may also be conducive to the development of stratiform clouds, in analogy with the low-level convection that forms over the North Atlantic when cold continental air from over the northeastern United States flows out over the warm waters of the Gulf Stream during winter. Using ship observations of total cloud amount, Deser and Wallace (1990) showed that climatological mean cloud cover is enhanced over the front relative to the cold equatorial waters. The clouds over the front are distinct from the deep convection along the intertropical convergence zone (ITCZ) to the north (Warren et al. 1988). A strong qualitative correlation between the front position and the occurrence of stratocumulus clouds was also noted by Bates (1986) on the basis of satellite measurements. The datasets used in these studies, however, did not allow for a detailed description of the spatial and temporal variability of the clouds over the front.

The intensity of the front varies on time scales ranging from weeks to years. The weekly variations are a result of tropical instability waves that cause the front to meander north and south (Legeckis 1977). Warm and cold events associated with the El Niño–Southern Oscillation cycle lead to interannual changes in the strength of the front. The purpose of this study is to document the association between stratiform cloud and SST variations along the equatorial front using high-resolution satellite measurements of SST and cloud reflectivity. The radiative impact of the clouds upon the front, which represents a negative feedback, is also examined.

The satellite measurements and data processing techniques are described in section 2. The association between SST and cloudiness variations along the front is documented in section 3. The radiative impact of

Corresponding author address: Dr. Clara Deser, University of Colorado, CIRES, Campus Box 449, Boulder, CO 80309.

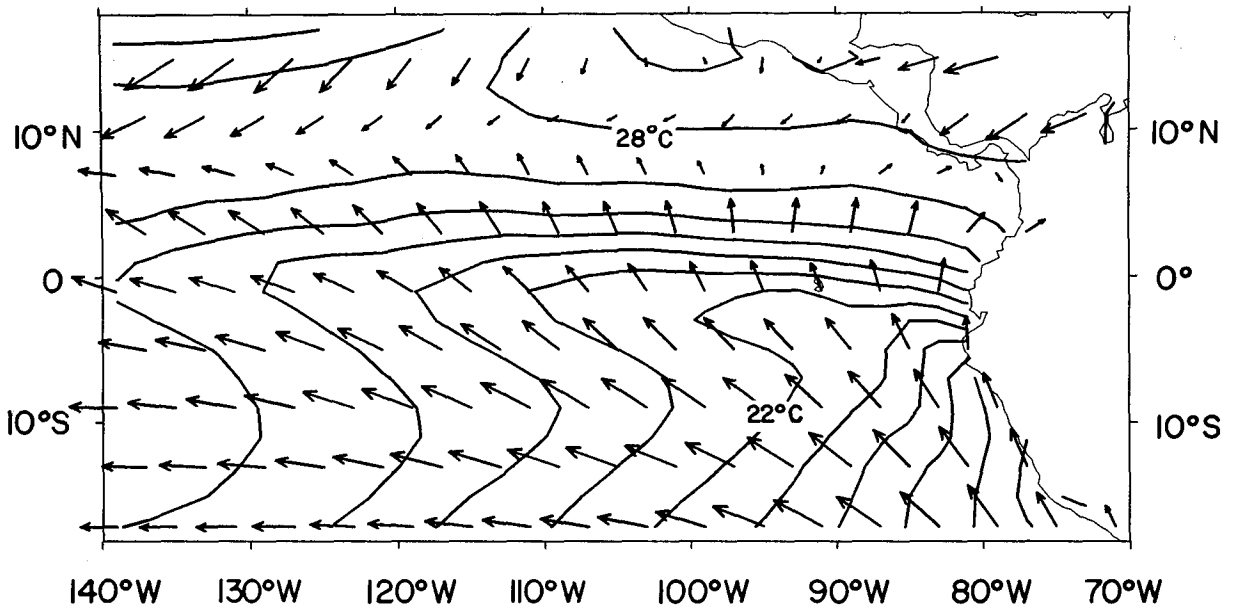

FIG. 1. Climatological mean distributions of SST (°C) and surface wind during July–November from the Comprehensive Ocean-Atmosphere Data Set, based on the period 1950–79. The longest arrow is 0.7 m s^{-1}. The contour interval for SST is 1°C.

the clouds upon SSTs is discussed in section 4. Summary and conclusions are given in section 5.

2. Data

a. Cloud

To study the interaction of clouds with the front, the International Satellite Cloud Climatology Project (ISCCP) reduced-resolution global radiance (B3) data were used. As described by Schiffer and Rossow (1985), Stage B3 data are a reduced-resolution version of the original geostationary satellite images produced by sampling in both time and space to a nominal spacing of 3 h and 30 km. An important part of ISCCP processing is the intercalibration of visible wavelength radiometers on different satellites (Rossow and Schiffer 1991). None of the current satellite visible radiometers have onboard calibration inflight. The ISCCP project normalizes the relative calibrations of all the polar orbiters and monitors them for long-term drifts during their lifetimes. Comparisons are made with the geostationary radiometers, and they are normalized to the polar orbiters. This permits long-term studies of radiance fields over specific regions independent of changes in satellites.

Following Schiffer and Rossow (1985), the original radiances, L (Wm^{-2} sr^{-1}), measured by the radiometer are expressed as normalized radiances, L^*, by dividing by the effective solar irradiance for that spectral region. Term L^* is then divided by the cosine of the zenith angle to give a bidirectional reflectance. Over the oceans under clear conditions, the reflectance is low and constant (outside of sunglint), and thus changes in bidirectional reflectance are directly related to changes in cloudiness. As discussed by Schiffer and Rossow (1985), there is no way to distinguish between changes in cloud reflectivity and changes in cloud amount with the ISCCP data. The reflectance data will be referred to as "visible cloudiness."

b. SST

As described in McClain et al. (1985), there are several different products generated within the framework of the multichannel sea surface temperature (MCSST) processing scheme. Raw MCSST retrievals are performed on 2 by 2 arrays of global area coverage (GAC) data from the advanced very high resolution radiometer (AVHRR/2) from the odd-numbered NOAA series of polar-orbiting satellites. The number of MCSST retrievals actually saved per target array of 11 by 11 GAC spots, however, varies geographically and between day and night. Typically, on the order of two million MCSST retrievals are made during one month. This is a somewhat cumbersome dataset for climate analysis and several reduced volume datasets are available for study. The product used here is a weekly average of daytime MCSST observations binned on an 18-km grid (generated by O. Brown; see Halpern et al. 1991, 1992). In this product, if clouds obscure a grid square for an entire week, no MCSST is retrieved. Even in regions of persistent cloudiness, however, there are enough cloud-free grid squares to define with confidence the underlying SST distribution (Bates and Diaz 1991). For the region of interest, no more than two adjacent

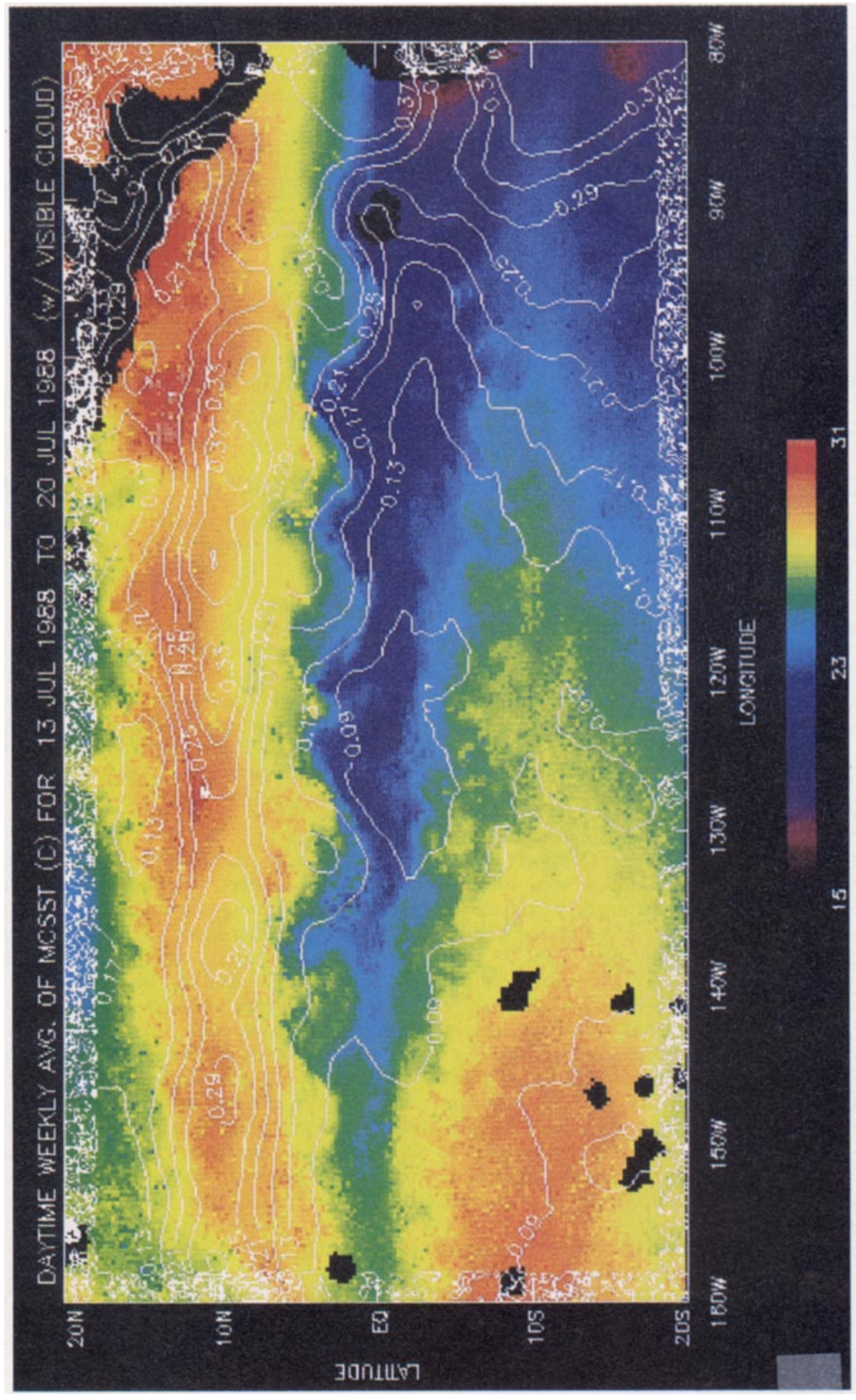

FIG. 2. Distributions of SST (colors) and visible cloud (contours; %) for 13–20 July 1988. The color scale for the SST image (°C) is shown below the figure.

grid squares were obscured by clouds in any given week. Spatial linear interpolation is used to fill in missing SST data.

In order to facilitate comparison of the cloud and SST datasets, each was interpolated to a common grid of 25 km × 25 km. ISCCP data from 2100 UTC (1200-LT in the eastern Pacific) were used; these data were weekly averaged for compatibility with the SST product. This study uses data from 1987 and 1988.

3. Results

a. *Tropical instability waves during June–November 1988*

Meridional current velocities in the upper ocean of the equatorial eastern Pacific exhibit a pronounced spectral peak at periods ~ 20–30 days (Halpern et al. 1988). These eddy motions are the signature of tropical instability waves, so-called because they result from the latitudinal shear instability between the South Equatorial Current and the North Equatorial Counter Current (Cox 1980; Philander et al. 1985). The eddy motions advect the background SST field, bringing cold water northward and warm water southward: hence their signature in the SST field along the equatorial front. By virtue of their ability to transport heat southward into the equatorial cold tongue, tropical instability waves act to diffuse the SST gradients across the equatorial front (Philander et al. 1986). The waves have a longitudinal wavelength of ~1000 km and travel westward at ~25–80 cm s^{-1} (Halpern et al. 1988). The waves were well developed in the summer and autumn of 1988 (Hayes et al. 1989).

Figure 2 shows the distributions of visible cloud and SST for 13–20 July 1988. There are pronounced waves in the SST field (amplitude ~ 2°–3°C) along the northern edge of the cold tongue. The cloud reflectivity field (contours) follows the SST waves, with higher reflectivities in the warm troughs relative to the cold crests. A slight upstream phase shift of the clouds relative to the SST troughs is evident. This may be due to the angle of the surface wind field relative to the wave front (a southeasterly wind crosses the wave front at right angles on the upwind face of the wave) and to the fact that the SST waves are somewhat steeper on the downwind face.

To illustrate the type of cloud associated with the SST waves, a visible satellite image (from the Defense Meteorological Satellite Program Optical Line Scan) for 2135 UTC 8 July 1988 is shown in Fig. 3. The SST wave front (as delineated by the 23°C isotherm) for 6–13 July 1988 is drawn for reference. Stratocumulus clouds occur in the wave troughs (note the similarity between these clouds and those off the west coast of South America); the brighter clouds along 10°N in the ITCZ are cumulonimbus.

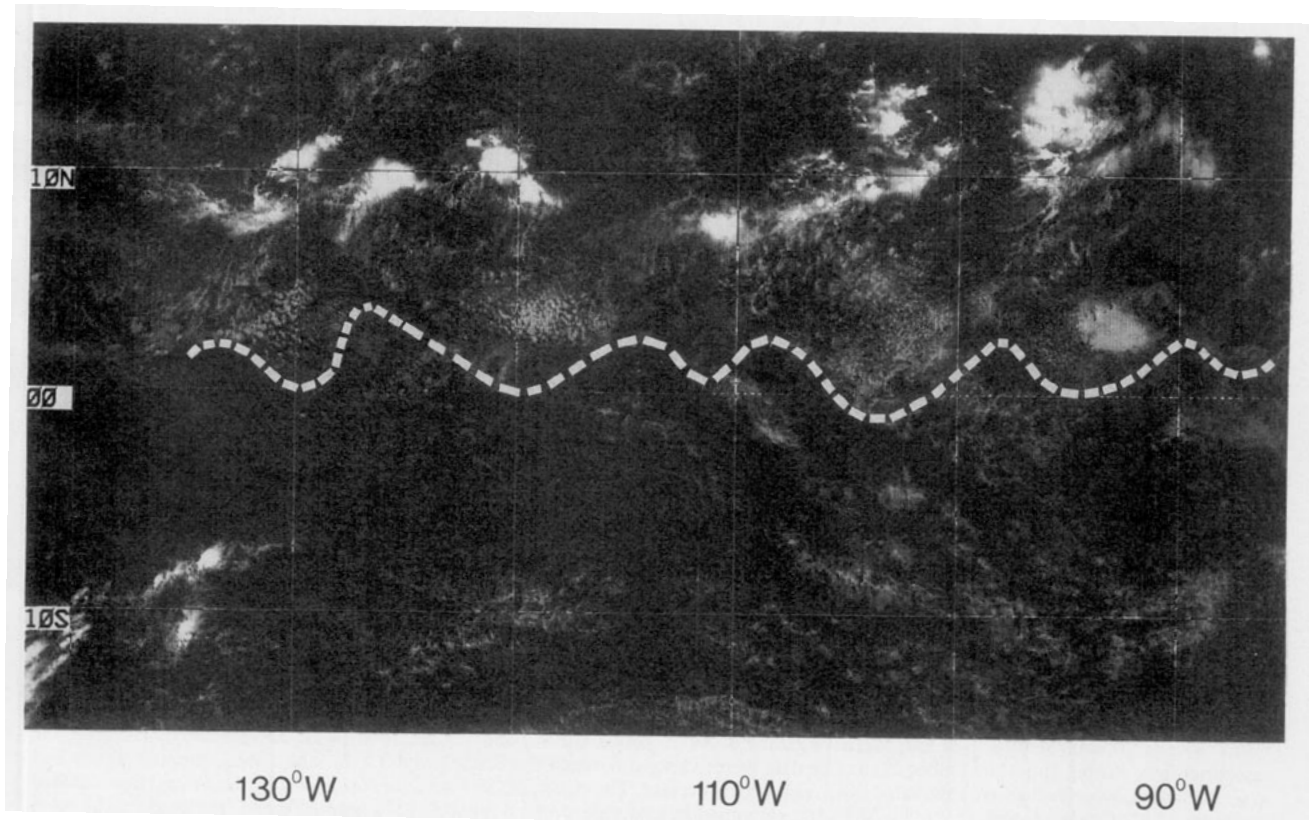

FIG. 3. Visible cloud image for 2135 UTC 8 July 1988. The SST wave front (as delineated by the 23°C isotherm) for the week of 6–13 July is drawn for reference.

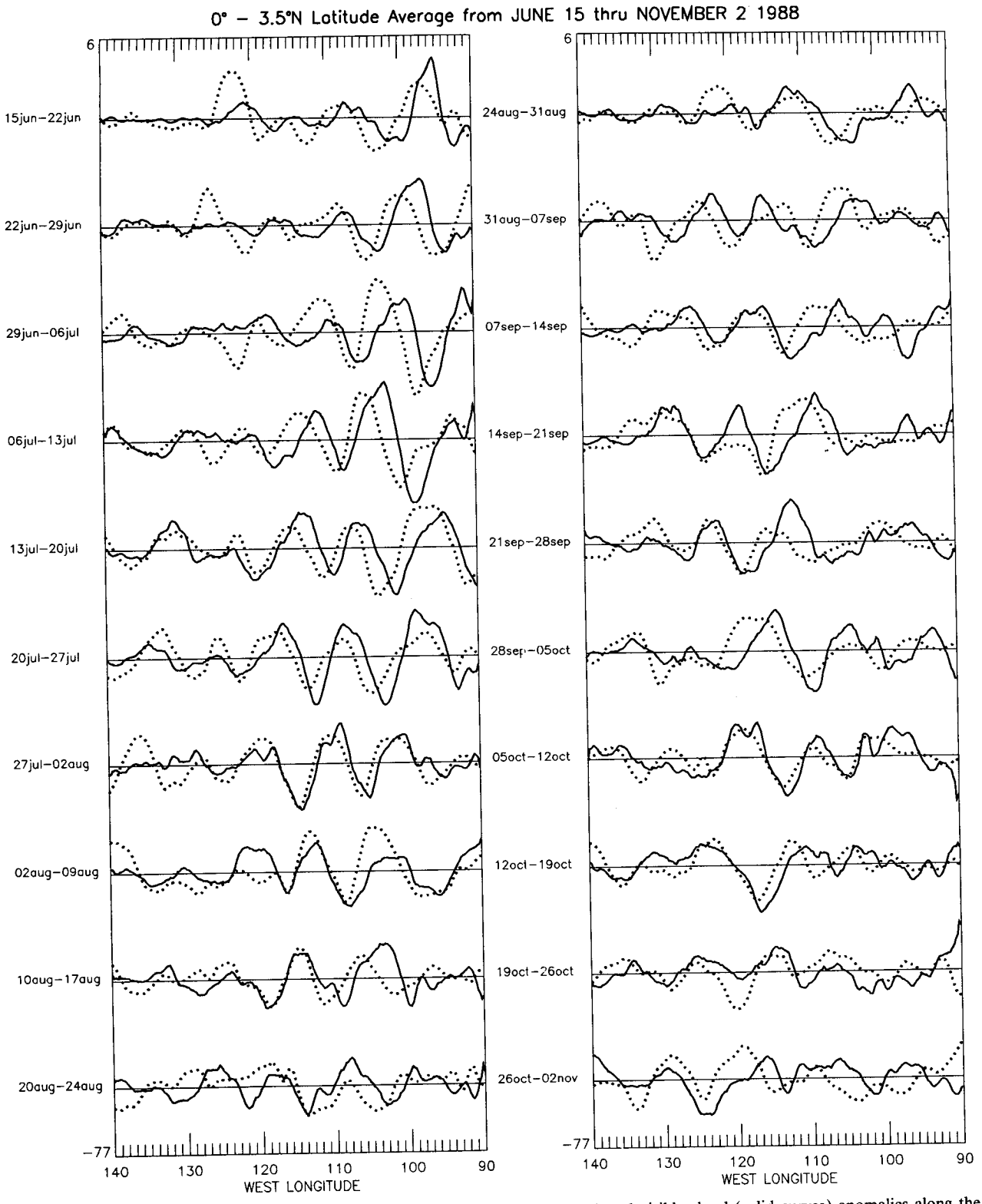

FIG. 4. The 20-week sequence of longitudinal sections of SST (dashed curves) and visible cloud (solid curves) anomalies along the equatorial front during June–November 1988. The data were averaged between the equator and 3.5°N. The 5-week running means and zonal least-squares parabolas were subtracted from each weekly average. The cloud and SST data are normalized by their respective standard deviations (2.9% for clouds and 0.55°C for SST) and smoothed in longitude with a 5-point (1.25°) running mean. The zero line for each week is marked by a horizontal line; the distance between successive zero lines is eight standard deviations.

Figure 4 shows a 20-week sequence of longitudinal sections of SST and visible cloud anomalies along the equatorial front during June–November 1988. The data were averaged between the equator and 3.5°N (the zone of largest SST variations associated with the waves) and smoothed in longitude with a five-point (1.25°) running mean. To enhance the signature of the waves, a five-week running mean and a zonal least-squares parabola were subtracted from each weekly average. Tropical instability waves are clearly apparent in the SST field; note that there is considerable fluctuation in their amplitude with time. The waves in the visible cloud field correspond closely to those in SST, with enhanced (reduced) cloudiness over and upstream of the positive (negative) SST anomalies. The cloud fluctuations weaken west of ~130°W relative to the SST waves. This may be due to the fact that the wind becomes progressively more easterly (e.g., parallel to the wave front) west of 130°W (Fig. 1).

The spatial correlation between the SST and visible cloud series shown in Fig. 4 (based on the longitude band 90°–130°W) is 0.54 at zero lag. The correlation rises to 0.80 when the SST series is lagged 1.25° west of the cloud series. Both correlation coefficients are statistically significant at the .01 level, using a one-tailed Student's t-test and taking into account the high degree of spatial autocorrelation in the smoothed series according to Leith (1973). The corresponding regression coefficient is 2.8% reflectivity per degree Celcius of SST at 0-lag (4.2% per °C at 1.25° lag). Thus, given a typical SST wave amplitude of 2.5°C, the corresponding cloud reflectivity amplitude is 7.1% (10.5% at 1.25° lag).

b. *Annual cycle*

Figure 5 shows the distributions of visible cloudiness (%) and brightness temperature (K; an indicator of deep convection) during September–October 1988 when the front and northward winds are near their seasonal maximum. In the visible cloud field (Fig. 5a), two distinct maxima are observed: one near 9°N associated with the ITCZ and one over the Equatorial Front east of 110°W. The brightness temperature distribution (Fig. 5b) shows only a single minimum near 9°N, confirming that the clouds over the front are low.

Meridional profiles of monthly mean visible cloudiness during 1988 for the longitude band 90°–110°W are shown in Fig. 6. The Northern Hemisphere ITCZ is evident throughout the year, migrating north and south with the sun. A Southern Hemisphere ITCZ appears briefly during February–April (this feature is not present every year). During July–November, a secondary visible cloud maximum occurs at 2°–3°N (i.e., over the equatorial front) when the front and northward winds are strongest. Note that the cloud reflectivity values over the front are comparable to those in the ITCZ during September–November.

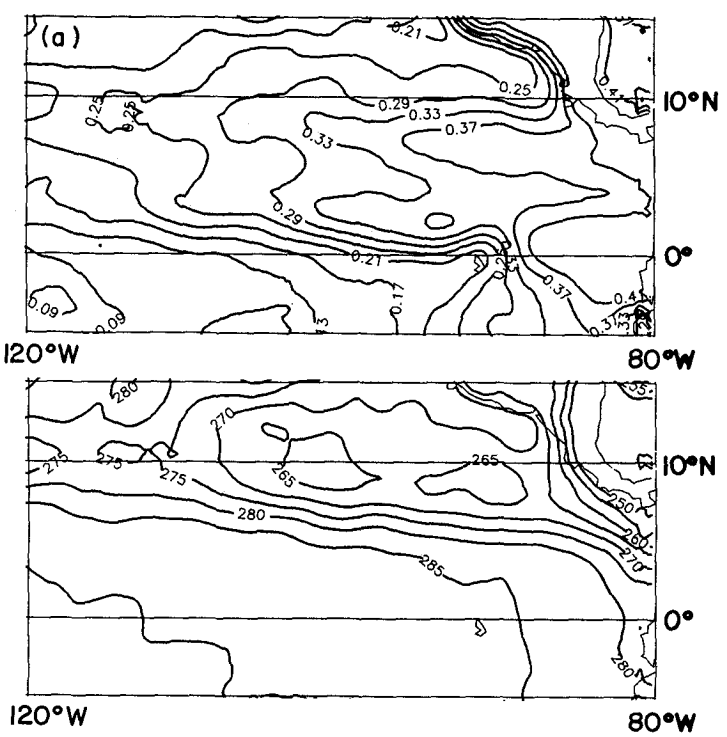

FIG. 5. Distributions of (a) visible cloudiness (%) and (b) brightness temperature (K; an indicator of deep convection) during September–October 1988.

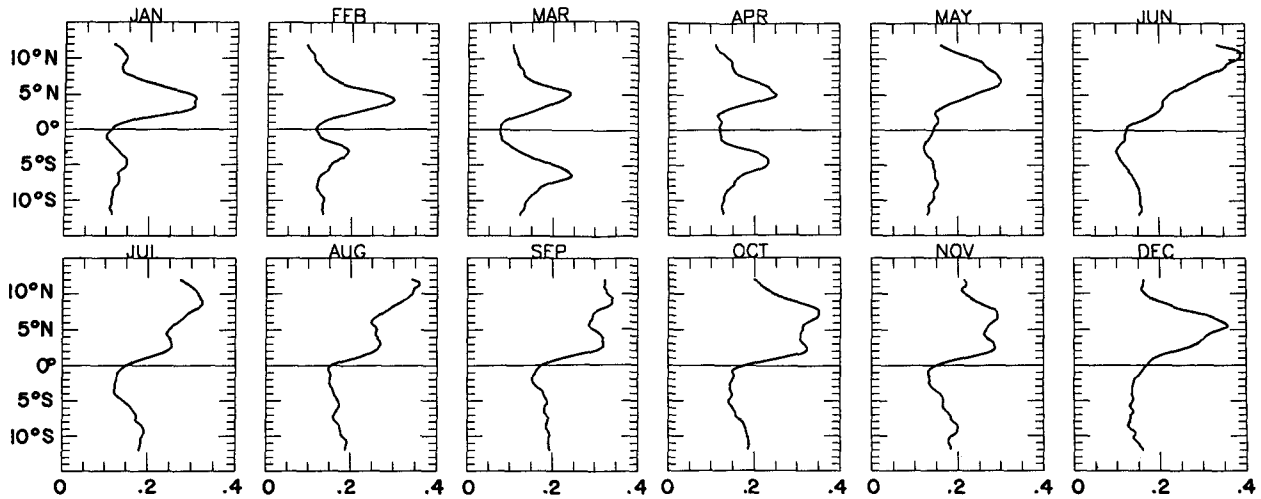

FIG. 6. Meridional profiles of visible cloudiness (%) for the longitude band 90°–110°W for each month during 1988.

c. Interannual variations

Figure 7 shows the distributions of visible cloud for September–October 1987 and 1988. The ITCZ convection was stronger and shifted southwards in 1987 relative to 1988. There was only a hint of enhanced cloudiness over the equatorial front in 1987. As shown in the right-hand panels, the SST gradient across the equatorial front during September–October was nearly twice as large in the cold year of 1988 as in the warm year of 1987. The distributions of visible cloud are consistent with these interannual changes in the strength of the front.

The latitudinal profile of the reflectivity difference

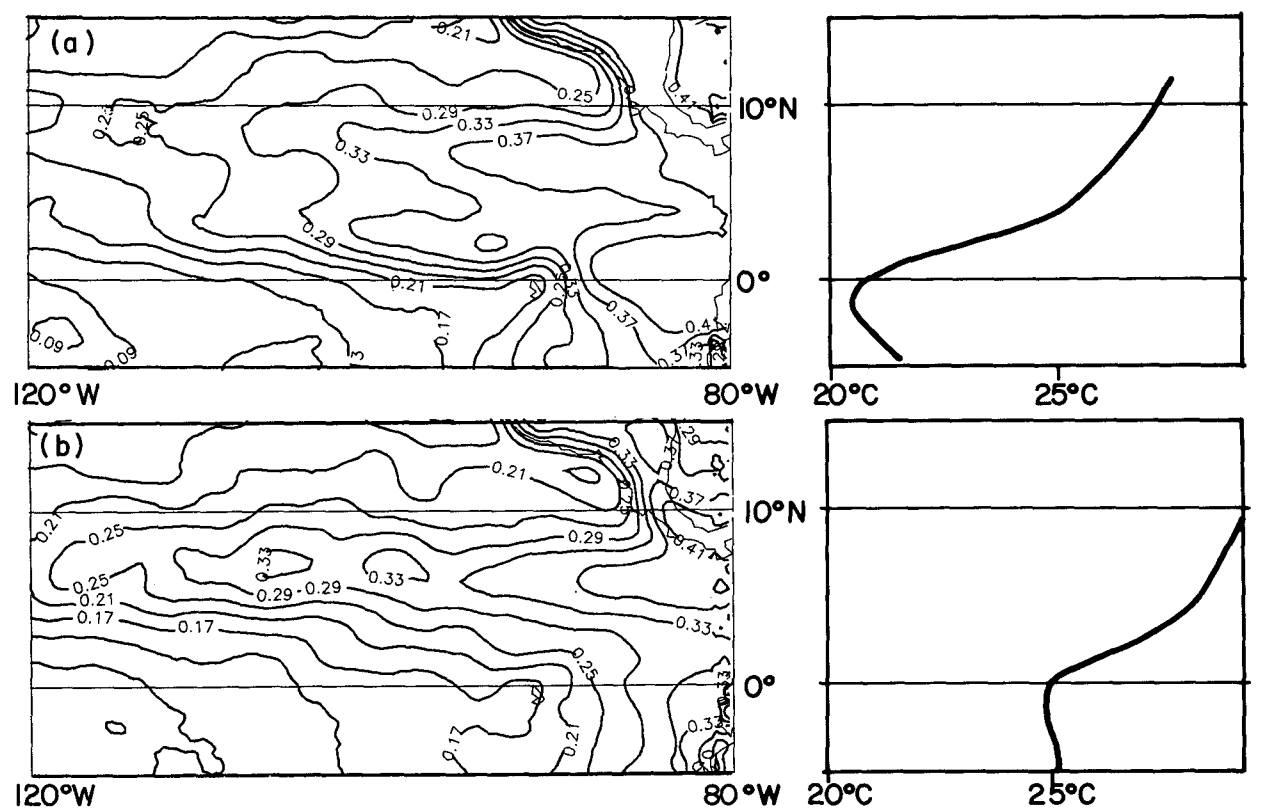

FIG. 7. Distributions of visible cloudiness (%) during September–October (a) 1988 and (b) 1987. Shown at right are the corresponding meridional profiles of sea surface temperature for the region 90°W–110°W.

between 1987 and 1988 for the region 90°W–120°W is shown in Fig. 8. The decrease in cloudiness from 1987 to 1988 at 2.5°N (10%) is much larger than the increase at 6°N (3%).

4. Impact of clouds upon the surface energy balance

The enhancement of clouds over the Equatorial Front and their suppression over the equatorial cold tongue will limit the SST gradients across the front by decreasing the incident solar radiation over the front relative to that over the cold tongue. In September–October 1988, the cloud reflectivity was 32.4% at 2.25°N and 16.0% at 0.5°S in the longitude band 90°–110°W (Fig. 6). Multiplying these reflectivities by the clear-sky insolation (from Seckel and Beaudry 1973) and taking into account the albedo of the sea surface (7%; Payne 1972) gives a 63 W m^{-2} change in incoming solar radiation across the front. Assuming the compensating longwave effect of the clouds is 15% (Breon et al. 1991), then the change in net radiation across the front is 54 W m^{-2}. This is about one-third of the change in the latent and sensible energy fluxes across the front, as estimated from the Comprehensive Ocean-Atmosphere Data Set (Woodruff et al. 1987; not shown). The meridional gradient in the total surface energy flux (radiative plus latent and sensible) across the front (200 W m^{-2}) is comparable to the southward heat flux effected by the oceanic instability waves (Halpern et al. 1988; Bryden and Brady 1989). Assuming a mean mixed-layer depth of ~20 m (estimated from buoy measurements at 2°N, 0°, 2°S at 110°W using the criterion that the temperature in the mixed layer is within 0.5°C of that at the sea surface), the surface energy fluxes would reduce the SST gradient across the front by a factor of $1/e$ in ~ one month.

The formation of low clouds in the warm troughs relative to cold crests of the tropical instability waves will tend to weaken the SST anomalies associated with the waves. It was shown above that for a typical SST wave amplitude of 2.5°C, the corresponding cloud reflectivity change is 7.1%. Multiplying the reflectivity change by the daily averaged clear-sky insolation (385 W m^{-2}) and assuming a sea surface albedo of 7% gives a 25 W m^{-2} change in solar radiation incident at the sea surface. Assuming that this radiation is distributed over a mixed-layer depth of 20 m, the resulting SST tendency is 0.75°C per month (0.64°C per month if the compensating longwave effect of the clouds is taken into account). The implied e-folding time scale (3 months) is long in comparison to the time scale of the waves.

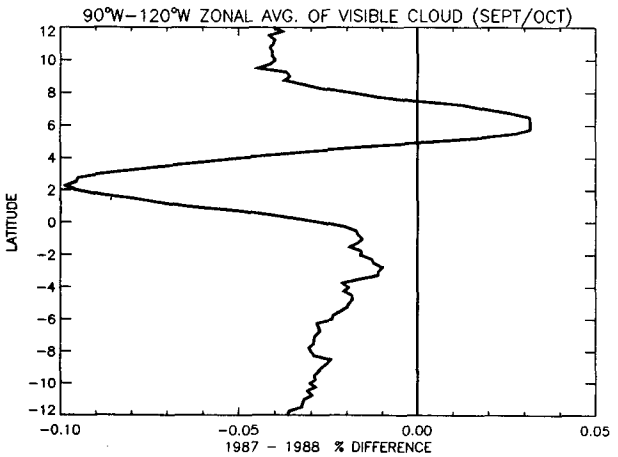

FIG. 8. Meridional profile of the September–October visible cloud difference (%) between 1987 and 1988 for the region 90°–120°W.

5. Conclusions

It was hypothesized that the configuration of cool low-level winds blowing across a sharp SST front in the eastern equatorial Pacific would give rise to low-level convection on the warm downstream side of the front. High-resolution satellite measurements of visible cloud and SST were used to test this idea. The results show that there is a maximum in visible cloudiness over the Equatorial Front during the cold season of 1988, when the front and northward winds were strong. The visible cloud maximum was reduced in the warm (El Niño) year of 1987, consistent with the weakening of the front. Instability waves along the equatorial front were pronounced during the summer and autumn of 1988. The results show a strong association between visible cloud and the SST waves, with enhanced (reduced) cloudiness in the warm troughs (cold crests) of the waves.

The kinematic and thermodynamic structure of the atmospheric planetary boundary layer exhibits a rich response to the underlying distribution of SST in the eastern equatorial Pacific. Low-level wind shear, surface wind speed, surface relative humidity, and air–sea temperature difference all exhibit transitions across the equatorial front (Bond 1922; Wallace et al. 1989; Hayes et al. 1989; Deser and Wallace 1990). This study has shown that the low-level cloudiness distribution is also sensitive to the underlying thermal structure. A field program designed to study the mechanism of cloud formation over the equatorial front would be a valuable complement to current experiments (e.g., FIRE[1]) that are directed toward understanding the widespread stratocumulus cloud decks over the cold subtropical eastern oceans.

Acknowledgments. We thank S. J. S. Khalsa, J. M. Wallace, and the official reviewers for their valuable comments. The ISCCP data were provided by Satellite

[1] First International Satellite Cloud Climatology Project Regional Experiment.

Data Services Division of NOAA/NESDIS. The MCSST data were provided by O. Brown and colleagues at the University of Miami through the NASA Ocean Data System at the Jet Propulsion Laboratory. This work was supported by the Equatorial Pacific Ocean Climate Studies (EPOCS) Program of NOAA.

REFERENCES

Bates, J. J., 1986: A technique to estimate the ocean surface heat flux using VAS multispectral data. Ph.D. dissertation, University of Wisconsin-Madison, 144 pp.

——, and H. F. Diaz, 1991: Evaluation of multichannel sea surface temperature product quality for climate monitoring: 1982–1988. *J. Geophys. Res.*, **96,** 20 613–20 622.

Bond, N. A., 1992: Observations of planetary boundary layer structure in the eastern equatorial Pacific. *J. Climate,* **5,** 699–706.

Breon, F.-M., R. Frouin, and C. Gautier, 1991: Downwelling longwave irradiance at the ocean surface: An assessment of in situ measurements and parameterizations. *J. Appl. Meteor.*, **30,** 17–31.

Bryden, H. L., and E. C. Brady, 1989: Eddy momentum and heat fluxes and their effects on the circulation of the equatorial Pacific Ocean. *J. Mar. Res.*, **47,** 55–79.

Cox, M. D., 1980: Generation and propagation of 30-day waves in a numerical model of the Pacific. *J. Phys. Oceanogr.*, **10,** 1168–1186.

Deser, C., and J. M. Wallace, 1990: Large-scale atmospheric circulation features of warm and cold episodes in the tropical Pacific. *J. Climate,* **3,** 1254–1281.

Halpern, D., R. A. Knox, and D. S. Luther, 1988: Observations of 20-day period meridional current oscillations in the upper ocean along the Pacific equator. *J. Phys. Oceanogr.*, **18,** 1514–1534.

——, V. Zlotnicki, J. Newman, O. Brown, and F. Wentz, 1991: An atlas of monthly mean distributions of GEOSAT sea surface height, SSMI surface wind speed, AVHRR/2 sea surface temperatures, and ECMWF surface wind components during 1988. JPL Publication 91-8, Jet Propulsion Laboratory, 110 pp.

——, ——, ——, D. Dixon, O. Brown, and F. Wentz, 1992: An atlas of monthly mean distributions of GEOSAT sea surface height, SSMI surface wind speed, AVHRR/2 sea surface temperatures, and ECMWF surface wind components during 1987. JPL Publication 92-3, Jet Propulsion Laboratory, 111 pp.

Hayes, S. P., M. J. McPhaden, and J. M. Wallace, 1989: The influence of sea surface temperature variability upon surface wind in the eastern equatorial Pacific: Weekly to monthly variability. *J. Climate,* **2,** 1500–1506.

Leith, C. E., 1973: The standard error of time-averaged estimates of climatic means. *J. Appl. Meteor.*, **12,** 1066–1069.

Legeckis, R. V., 1977: Long waves in the eastern tropical Pacific Ocean: A view from a geostationary satellite. *Science,* **197,** 1179–1181.

McClain, E. P., W. G. Pichel, and C. C. Walton, 1985: Comparative performance of AVHRR-based sea surface temperatures. *J. Geophys. Res.*, **90,** 11 587–11 601.

Payne, R. E., 1972: Albedo of the sea surface. *J. Atmos. Sci.*, **29,** 959–970.

Philander, S. G. H., D. Halpern, D. Hansen, R. Legeckis, M. Laury, C. Paul, D. Watts, R. Weisberg, and M. Wimbush, 1985: Long waves in the equatorial Pacific Ocean. *Trans. Amer. Geophys. Union,* **66,** 154.

——, W. J. Hurlin, and R. C. Pacanowski, 1986: Properties of equatorial long waves in models of the seasonal cycle in the tropical Atlantic and Pacific oceans. *J. Geophys. Res.*, **91,** 14 207–14 211.

Rossow, W. B., and R. A. Schiffer, 1991: ISCCP cloud products. *Bull. Amer. Meteor. Soc.*, **72,** 2–20.

Schiffer, R. A., and W. B. Rossow, 1985: ISCCP global radiance dataset: A new resource for climate research. *Bull. Amer. Meteor. Soc.*, **66,** 1498–1505.

Seckel, G. R., and F. H. Beaudry, 1973: The radiation from sun and sky over the North Pacific Ocean, Abstract. *Trans. Amer. Geophys. Union,* **54,** 1114.

Wallace, J. M., T. P. Mitchell, and C. Deser, 1989: The influence of sea surface temperature variability upon surface wind in the eastern equatorial Pacific: Seasonal and interannual variability. *J. Climate,* **2,** 1492–1499.

Warren, S. G., C. J. Hahn, J. London, R. M. Chervin, and R. L. Jenne, 1988: Global distribution of total cloud cover and cloud type amounts over the ocean. NCAR Tech. Note, TN-317+STR, 44 pp + 170 Figs.

Woodruff, S. D., R. J. Slutz, R. L. Jenne, and P. M. Steurer, 1987: A comprehensive ocean-atmosphere dataset. *Bull. Amer. Meteor. Soc.*, **68,** 521–527.